



## OPTICS

# Quantum and coherent signal transmission on a single-frequency channel via the electro-optic serrodyne technique

Philip Rübeling<sup>1†</sup>, Jan Heine<sup>1†</sup>, Robert Johanning<sup>1,2</sup>, Michael Kues<sup>1,2\*</sup>

Fiber-optical networks are well established to accommodate global data traffic via coherent information transmission. The next generation of telecommunications will require the integration of quantum information into fiber-optic networks, e.g., for quantum key distribution. A promising and scalable route to enable quantum networking is encoding quantum information into the frequency of photons. While the cointegration of frequency-entangled photons with coherent information transmission is achieved via spectral multiplexing, more resource-efficient approaches are required. In this work, we introduce and experimentally demonstrate a transceiver concept that enables the transmission of coherent and frequency-entangled photons over a single-frequency channel. Our concept leverages the serrodyne technique via electro-optic phase modulation leading to very different dynamics for entangled and coherent photons. This enables temporal multiplexing of the respective signals. We demonstrate the preservation of entanglement over the channel in the presence of coherent light. Our approach reveals a strong potential for efficient bandwidth use in hybrid networks.

Copyright © 2024 the Authors, some rights reserved; exclusive licensee American Association for the Advancement of Science. No claim to original U.S. Government Works. Distributed under a Creative Commons Attribution NonCommercial License 4.0 (CC BY-NC).

## INTRODUCTION

Quantum networks (1, 2) are the backbone of quantum technologies such as quantum communications (3) and distributed quantum computing (4, 5) with the purpose to broadcast entanglement among remote parties separated by hundreds of kilometers (6). It is likely that quantum networks will be the key enabler for advanced quantum networking protocols with a broad impact on the next generation of information technology. Two primary approaches exist to establish quantum networks. The first involves the utilization of spatially manipulated photons (7) within frameworks reliant on free-space optics. The second approach centers on systems based on optical fiber, wherein different degrees of freedom, such as frequency, time, polarization, etc., are harnessed.

Encoding quantum information into the frequency of photons is particularly promising to implement large-scale fiber-based quantum networks (8, 9). Unlike the polarization of a photon, this degree of freedom is scalable to high-dimensional quantum states (so-called qudits) (10, 11), hyper-entangled quantum states (12), and compatible with existing telecommunications infrastructure and chip fabrication. In addition, fully integrated sources of frequency qudits and photonic elements for coherent control have proven to be scalable (13, 14) and become increasingly accessible through photonic integration (15, 16).

Special attention is devoted to the potential synergies of telecommunications infrastructure and quantum networks. Previous work demonstrated spectral multiplexing of entangled photons (17, 18) and simultaneous operation of quantum key distribution and coherent communication protocols over the same fiber link (19, 20). The major advantage of these hybrid quantum coherent networks is the use of preexisting telecommunication infrastructure, without the

need for additional fiber deployment. This approach is in line with the cointegration of quantum frequency combs (21) and coherent frequency combs (22, 23) in integrated photonic circuits. In addition, dynamic channel allocation can balance quantum and coherent signal transmission specifically tailored to the needs of users connected to the link. However, all hybrid networks implemented so far are based on a single-fiber multi-channel architecture, i.e., frequency channels in the O, L, and C bands are identified either for coherent or quantum signals. As we outline in this work, separate frequency channels for quantum and coherent signals are not required. Our work introduces a transceiver concept—the serrodyne transceiver—which enables transmission of frequency-entangled photons and a coherent signal on a single-frequency channel via efficient temporal multiplexing by exploiting the signals' different serrodyne dynamics.

The serrodyne technique applies a linear temporal phase ramp to translate the spectrum of an optical pulse. According to Fourier theory, this spectral shift  $\Delta\nu$  is proportional to the instantaneous frequency (or slope) of the phase applied (see the Supplementary Materials). The serrodyne technique has been demonstrated in acousto-optical (24, 25) ( $\Delta\nu \sim 3$  GHz), opto-mechanical (26) ( $\Delta\nu \sim 150$  GHz), electro-optical (27) ( $\Delta\nu \sim 640$  GHz), and all-optical (28, 29) ( $\Delta\nu \sim 10$  THz) platforms opening up seamless spectral manipulation for coherent and quantum light. Electro-optical phase modulation is especially suited for the manipulation of signals in the C band as the spectral translations are comparable with the channel spacings ( $\sim 12.5$  to  $\sim 200$  GHz) used in dense-wavelength division multiplex (DWDM) technology (30). Previous work on electro-optical phase modulation of quantum light focused on the spectral dynamics of frequency-separable photons generated by spontaneous parametric down conversion (SPDC) in type-II phase-matched  $\chi^{(2)}$  materials. This included electro-optical manipulation schemes such as the serrodyne technique (31) and spectral bandwidth compression of frequency-separable photons (32, 33), which have a well-defined temporal pulse shape. However, frequency-entangled photons, showing temporally delocalized dynamics, are required to

<sup>1</sup>Institute of Photonics (IOP), Leibniz University Hannover, Nienburger Straße 17, 30167 Hannover, Germany. <sup>2</sup>Cluster of Excellence PhoenixD (Photonics, Optics, and Engineering - Innovation Across Disciplines), Leibniz University Hannover, Welfengarten 1, 30167 Hannover, Germany.

\*Corresponding author. Email: michael.kues@iop.uni-hannover.de

†These authors contributed equally to this work.

implement quantum protocols and quantum network applications in the frequency domain (34, 35).

## RESULTS

The operational principle of our transmitter-receiver system is schematized in Fig. 1. A typical scenario involves two parties—Alice and Bob—having access to the same frequency channel of an optical fiber link. This channel serves the dual purpose of transmitting coherent signals and distributing entanglement across Alice and Bob. To do so, Alice generates a pair of frequency-entangled photons, which is demultiplexed into signal and idler photon. Subsequently, Alice performs a measurement on the signal photon, while the idler photon is directed toward the transmitter. Here, the idler photon is spectrally multiplexed with a pulsed coherent signal of an adjacent frequency channel through a DWDM filter (200 GHz) in add-configuration.

Subsequently, both signals are routed to an electro-optic phase modulator. Here, different dynamics arise because of the distinct temporal coherence times of the respective signals (see below). The coherent signal is translated by 200 GHz, while the stream of entangled photons remains largely unmodulated; see Fig. 2. The combined signals, coexisting within a 200-GHz frequency channel, are then forwarded to the optical fiber link. By transmitting both signals

on a single-frequency channel, the required optical bandwidth on the transmission line is reduced by a factor of 2. At Bob's receiver, the coherent signal is spectrally separated from the entangled photons by another electro-optic phase modulator reversing the frequency shift. A second DWDM filter in drop-configuration yields access to the idler photon, entangled with Alice's photon, as well as the coherent signal. The transceiver is symmetric and thus suited for bidirectional hybrid transmission.

To optically transmit classical information, our technique demands coherent return-to-zero signals such as those generated by an ultrashort pulsed laser. Encoding classical information onto return-to-zero signals can be achieved, e.g., via amplitude modulation. When operated in hybrid mode, a fundamental trade-off exists between the quantum and coherent channel capacity, due to the temporal overlap of the quantum and coherent signal on the 200-GHz channel. The portion of the quantum signal that has temporal overlap with the coherent signal [and therefore the radio frequency (RF) waveform] is shifted in the same direction as the coherent signal. The respective channel capacities can be controlled, e.g., by changing the laser and RF waveform repetition rate.

Serrodyne dynamics are well-understood for coherent laser pulses (36). We show that different serrodyne dynamics emerge for frequency-entangled photons due to their random arrival time with

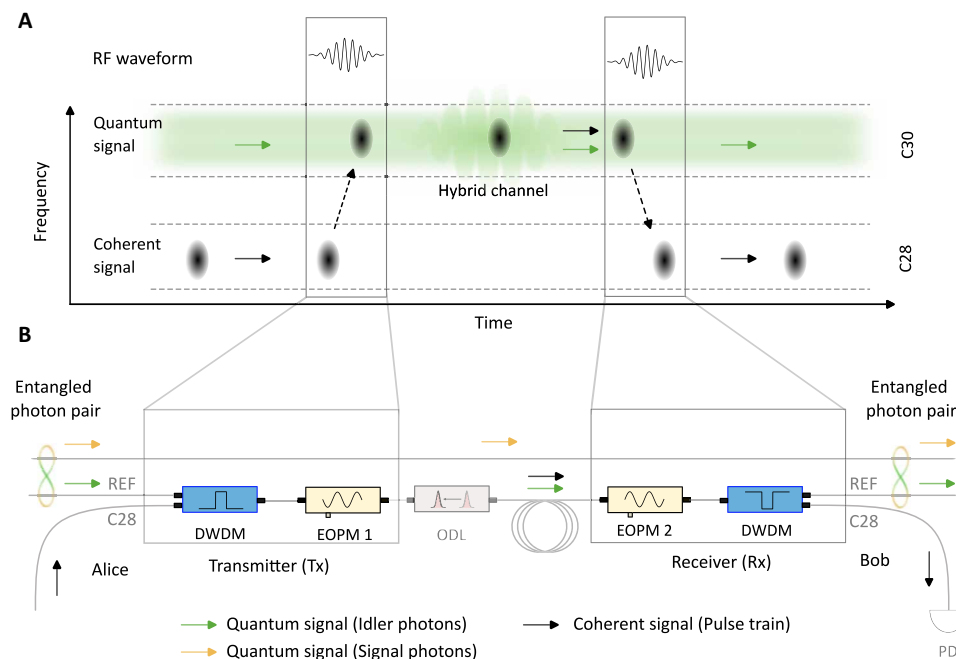


**Fig. 1. Operational principle and schematic setup of the serrodyne transceiver.** (A) The serrodyne transceiver concept is presented in the time-frequency domain. On the transmitter side, a train of coherent pulses (black) is incident on a 200-GHz frequency channel (C28). The adjacent frequency channel (C30) is populated by a stream of entangled photons (green). When subjected to phase modulation (gray boxes), quantum and coherent signals undergo different spectral dynamics due to their distinct temporal characteristics with respect to the radio frequency (RF) waveform. Coherent pulses coincide with the RF waveform and are shifted onto the frequency channel of the entangled photons (black dotted arrow). In contrast, frequency-entangled photons have a random arrival time with respect to the RF waveform due to their random time of generation in the SPDC process. Therefore, frequency-entangled photons that do not temporally coincide with the pulsed RF waveform are not shifted in frequency. As a result, quantum and coherent signals can coexist on channel C30. On the receiver side, the coherent pulse is shifted back onto its original frequency channel separating and recovering the signals. (B) Schematic setup of the electro-optic serrodyne transceiver, consisting of the transmitter and the receiver (gray boxes), each built from a DWDM filter and an electro-optical phase modulator (EOPM). The quantum signal consists of frequency-entangled idler photons (green arrows) and signal photons (orange arrows) generated from a parametric source. The idler photons are sent through the transmitter. The coherent signal is generated by an attenuated, pulsed laser, injected into the transceiver and read out on a photodetector (PD). The relative time delay between coherent pulses and the RF waveforms is adjusted by a variable optical delay line (ODL). More details on the experimental setup are provided in the Supplementary Materials.

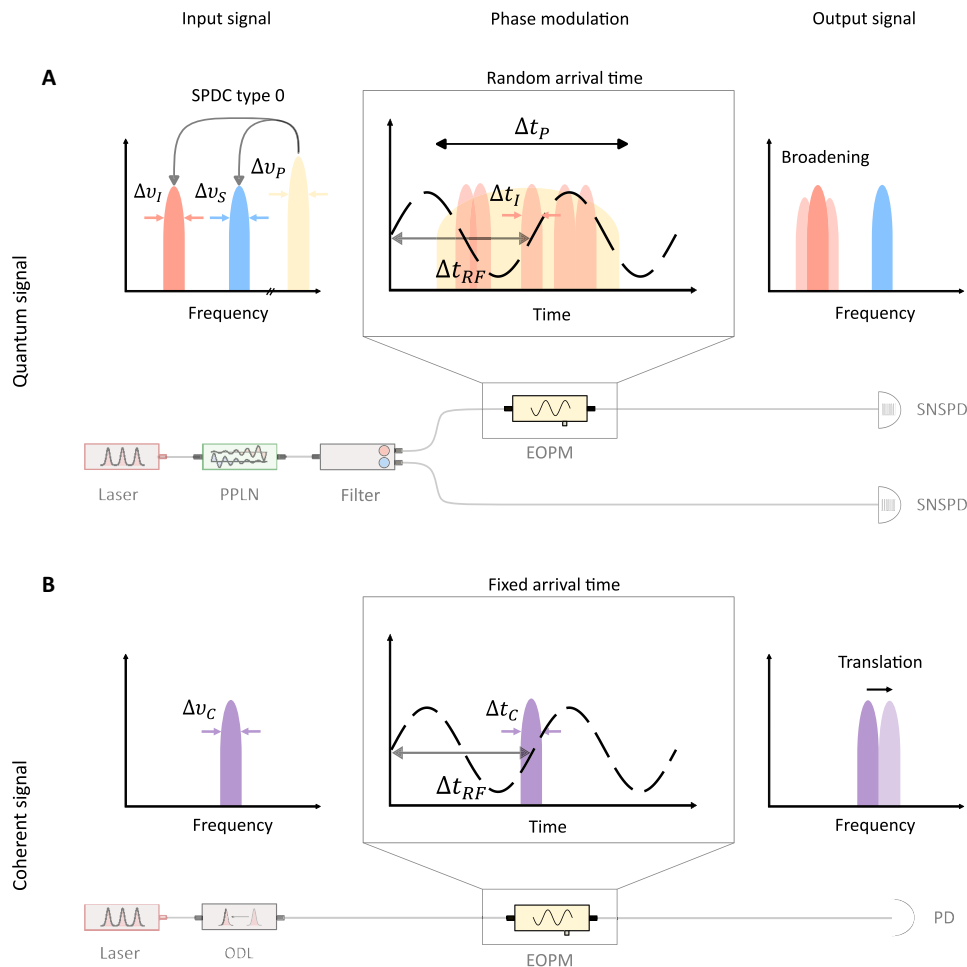


**Fig. 2. Time and frequency scales of the serrodyne dynamics. (A)** A narrow bandwidth pump field  $\Delta v_P = 7.1$  GHz (pulse duration  $\Delta t_P = 2$  ns) is used to excite the SPDC process. The pulse duration of the individual photons  $\Delta t_i$  depends on the single-photon bandwidth  $\Delta v_i = 80$  GHz. If the spectral bandwidth of the pump field is narrower than the single-photon bandwidth, as it is in our case, the photon pairs are created at random times within the temporal envelope of the pump pulse. Such condition results in a random arrival time of the photon pairs with respect to the RF waveform if the pump pulse duration is longer than the RF periodicity ( $\Delta t_{RF} = 50$  ps). Because of the random arrival time, various segments of the RF waveform with different slope are sampled, resulting in an overall broadening of the spectrum. Note that only the idler photon is modulated. **(B)** Coherent pulses with a large bandwidth  $\Delta v_C = 80$  GHz, whose temporal pulse length  $\Delta t_C$  is short compared to the temporal RF periodicity  $\Delta t_{RF}$ , have a fixed temporal relationship to the RF waveform. The coherent pulses therefore always coincide with the rising or falling edge of the RF waveform and are spectrally translated.

respect to the RF waveform. Serrodyne dynamics comparable to the ones of frequency-entangled photons are obtained for incoherent laser noise (e.g., amplified spontaneous emission), which does not exhibit a fixed temporal relationship with respect to the RF waveform (see the Supplementary Materials). We exploit the difference in the dynamics to perform distinct spectral transformations of the coherent light and entangled photons, enabling the hybrid transceiver operation; see Fig. 2. A comparable effect was used in demonstrating coherent denoising (37, 38), where different coherence times were exploited to separate a coherent signal from incoherent noise.

As a starting point, we filtered coherent light pulses with a Gaussian envelope (80-GHz 3-dB bandwidth) from the spectrum of a mode-locked femtosecond laser with its repetition rate (50 MHz) harmonically locked to a 1-GHz reference signal from an arbitrary waveform generator (AWG) via a phase-locked loop. These pulses fully fit inside the available channel bandwidth of 200 GHz at 192.8 THz

(C28). In a good approximation, the temporal length of these pulses (Fourier-limit corresponding to 5.5 ps) was about 11% of the total RF waveform length (50 ps, 20-GHz sinusoidal RF waveform) that we applied for modulation. This condition ensured that the optical pulse overlaps the RF signal in the linear segment, and aberrations due to parabolic contributions are minimized. We adjusted the relative phase delay between the RF waveform and the optical pulses by a variable optical delay line to address the falling edge (red detuning) or rising edge (blue detuning) of the sinusoidal RF waveform, respectively.

Pairs of frequency-entangled photons were prepared from the SPDC continuum of a type-0 phase-matched periodically poled lithium niobate waveguide pumped by 775-nm pulses of 2-ns duration (7.1-GHz pump bandwidth) with 50-MHz repetition rate. We filtered the single-photon input to the transceiver symmetrically to the degeneracy point by a programmable filter. For the signal photons, a rectangular frequency filter (160-GHz bandwidth) was chosen and

the photons were routed to a superconducting nanowire single-photon detector (SNSPD) to herald the arrival of idler photons. The idler photons were shaped by a Gaussian filter (80-GHz 3-dB bandwidth) and subsequently propagated through the transceiver setup. To perform spectral analysis of the single photons, we set up a heralded single-photon spectrometer, scanning the filter frequency with a resolution of approximately 10 GHz via a programmable filter over a range of 600 GHz (see the Supplementary Materials). The same spectrometer was used for the detection of the coherent pulses.

To characterize the relevant features of the serrodyne transceiver, we measured the spectral dynamics for coherent optical pulses and for frequency-entangled photons. For this, we effectively recorded spectra at three relevant positions by enabling and disabling electro-optic phase modulators in our experiment. For the input spectrum (Alice), we disabled both modulators. For the spectrum between the transmitter and receiver (transmission line), we enabled the modulator

on the transmitter's side. For the output spectrum (Bob), we enabled both modulators. This scheme maintained comparable conditions, including optical loss, polarization, delays, etc.

Figure 3 (A to C) shows the spectral dynamics of coherent pulses and frequency-entangled photons for a sinusoidal RF waveform with a carrier frequency of 20 GHz. For coherent pulses, we obtained a frequency redshift of  $\Delta\nu_R = (-154.8 \pm 0.2)$  GHz and a blueshift of  $\Delta\nu_B = (155.4 \pm 0.3)$  GHz, respectively; see Fig. 3B. In contrast, the frequency-entangled photons undergo bimodal spectral broadening, showing different dynamics. This is a consequence of the random arrival time of the photons with respect to the RF waveform. The reversibility of the spectral dynamics, which is needed to recover the signals, is demonstrated in Fig. 3C, proving that the unitary manipulation of the first modulator can be compensated by a second modulator. The measurements were in excellent agreement with our numerical simulations (see the Supplementary Materials).

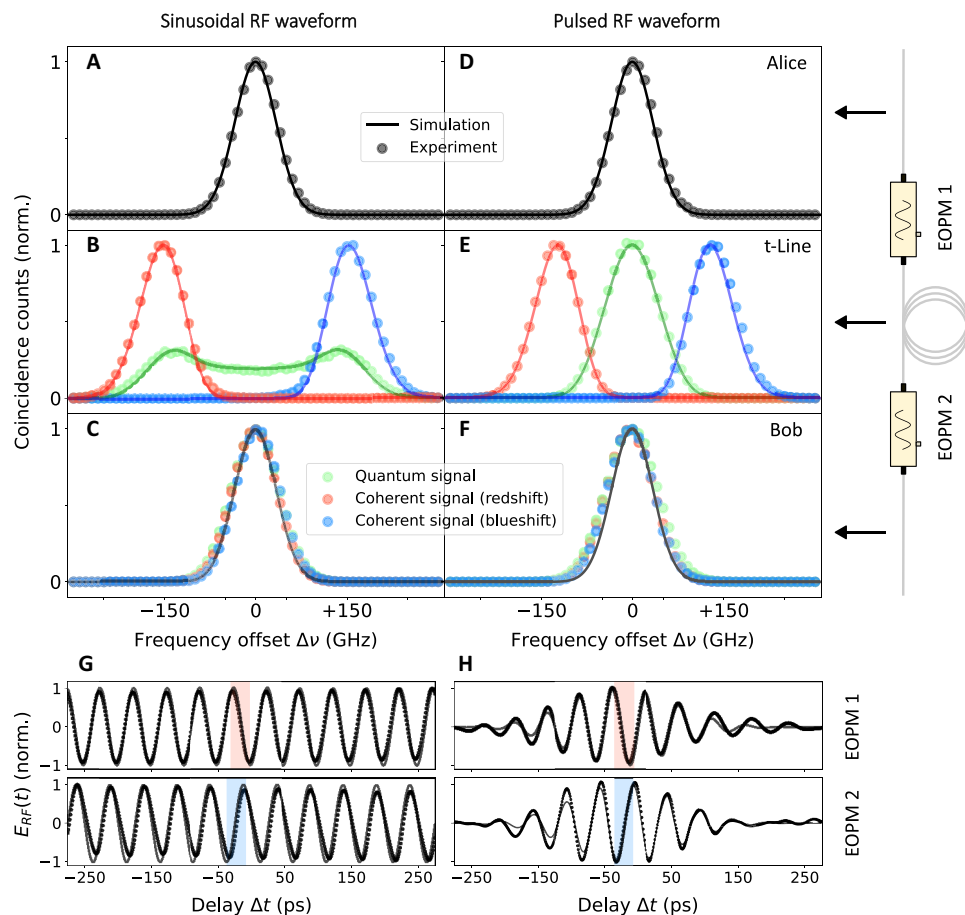


**Fig. 3. Spectral dynamics of the coherent signal and entangled photons measured at three positions, i.e., Alice, transmission line, Bob, of the transceiver for sinusoidal and pulsed RF waveforms.** (A) The input spectrum of coherent pulses and frequency-entangled photons follows a Gaussian shape. (B) For the sinusoidal waveform, coherent pulses (red and blue dots) are detuned by approximately  $\pm 150$  GHz in excellent agreement with our numerical simulations (solid red and blue lines). For frequency-entangled photons (green dots), the electro-optic interaction leads to bimodal spectral broadening in excellent agreement with our numerical result (solid green). (C) Modulation with the sign-inverted waveform at the second modulator restores the initial spectral shape of the coherent pulses at the output. A slight red detuning ( $< 10$  GHz) results from the imperfect optical delay match between the phase modulators. (D and F) Input and output spectra were the same as for sinusoidal RF waveforms. (E) For the pulsed RF waveform, a substantially reduced spectral broadening ( $\sim 18$ -GHz additional 3-dB-bandwidth) was observed for the frequency-entangled photons (green dots), in line with our numerical simulations (solid green line). (G and H) Experimentally reconstructed RF waveforms applied to the transmitter ( $\sim 303$  ps full-width at half maximum, EOPM1) and to the receiver ( $\sim 271$  ps full-width at half maximum, EOPM2). Differences in the pulsed waveforms arose from the accumulated response of the RF components. The black solid lines show the RF waveform set on the AWG. To obtain a maximal frequency shift with the pulsed RF waveform, we aligned the optical delay of the coherent pulses to the segment of highest positive/negative slope (blue/red shading).

The sinusoidal waveform is not ideal for operating the transceiver as the frequency-entangled photons should ideally remain in their frequency channel without notable spectral broadening. To address this issue, we determined an ideal RF waveform (see the Supplementary materials), which is a pulsed linear phase ramp, with the repetition rate synchronized to the optical pulse arrival time and duration as short as the coherent optical pulse ( $\sim 10$  ps). As a result, the photons remain on their initial frequency channel. Because of the bandwidth limitations of our system ( $< 28$ -GHz analog bandwidth), we approximated this signal by a pulsed RF waveform with 20-GHz carrier frequency (see Materials and Methods). To optimize and precompensate the waveforms, we reconstructed them using electro-optical sampling; see Fig. 3 (G and H) (see the Supplementary materials).

As demonstrated in Fig. 3 (D to F), the spectral distribution of the frequency-entangled photon remained preserved when the pulsed RF waveform is applied. For coherent pulses, we obtained a frequency redshift of  $\Delta\nu_R = (-128.7 \pm 0.4)$  GHz and a blueshift of  $\Delta\nu_B = (127.2 \pm 0.3)$  GHz, respectively, for this ideal waveform; see Fig. 3E. Again, as shown in Fig. 3F, the modulation with this RF waveform was reversible. Independent of the RF waveform used for modulation, a stable phase relationship between the RF waveforms and the optical signals is essential. In our experiments, this was ensured by the generation of the RF waveforms from independent channels of a single RF source with low interchannel jitter. As we used less than 6 m of fiber between transmitter and receiver, thermal length fluctuations of fibers were negligible ( $< 100$  fs). To achieve insensitivity to thermal length fluctuations that are inherent to longer fiber links, a remote phase synchronization between the RF sources generating the waveforms can be achieved for all frequency channels simultaneously by transmitting a synchronization signal via RF over fiber (39–41).

Our results of the hybrid transmission of coherent light and frequency-entangled photons with the serrodyne transceiver are shown in Fig. 4. At the transmitter side, coherent pulses with Gaussian shape (80-GHz 3-dB bandwidth, centered at 192.8 THz) were attenuated and multiplexed with the stream of entangled photons (80-GHz 3-dB bandwidth, centered at 193.0 THz) by a 200-GHz DWDM filter (C28,  $> 90$ -dB isolation) in add-configuration. The coherent photon flux at the transmitter input is estimated to be 146-times stronger than the entangled photon flux (see the Supplementary Materials). The spectrum of the combined signal at the input is shown in Fig. 4A. Note that the 146-fold signal amplitude cannot be reproduced by this measurement due to the fact that the coherent signal was post-selected conditioned on the heralding photon (see the Supplementary Materials). Subsequently, we propagated the multiplexed hybrid optical signal to the transmitter. After modulation, the coherent pulses were blue-shifted by 127.6 GHz; see Fig. 4B. A substantial part of the quantum ( $> 83\%$ ) and the coherent signal ( $> 95\%$ ) is in a spectral range of 200 GHz around 192.95 THz (H29), detected with our single-photon spectrometer. This demonstrates the single-frequency-channel multiplexing capabilities of our approach. A frequency shift of 200 GHz fully compatible with the 200-GHz international telecommunication union (ITU) grid could simply be achieved with a broadband RF amplifier system with a higher output power ( $> 35$  dBm saturation power) or conversely with an electro-optic phase modulator with lower half-wave voltage. As shown in Fig. 4C, we achieved a remarkable compensation of the serrodyne shift with the electro-optic phase modulator on the receiver

side by applying the sign-inverted pulsed RF waveform. This allowed us to recover both quantum and coherent signal after the modulator.

To demonstrate the proper operation of the established hybrid quantum coherent channel for applications in quantum information technology, we show that the serrodyne technique preserves entanglement of the quantum signal in the presence of a coherent signal. To prove the entanglement of the photons before and after the transmission through the transceiver, we performed quantum state tomography (see the Supplementary Materials) to reconstruct the density matrices at the input and output of the transceiver; see Fig. 4 (D and E, respectively). The input state generated by the SPDC process shows fidelity of  $F = (95.4 \pm 0.8)\%$  with respect to the Bell state, verifying the generation of the maximally frequency-entangled state from the SPDC process. Moreover, we calculated the Clauser-Horne-Shimony-Holt (CHSH) parameter  $S = (2.63 \pm 0.01)$  for the reconstructed input quantum state, violating the bound for local hidden-variable theories of  $|S| > 2$  (42). The output state from the transceiver under hybrid operation shows a fidelity of  $F = (89.6 \pm 1.7)\%$  with a CHSH-parameter of  $S = (2.58 \pm 0.06)$ , still violating the entanglement bound. Our results demonstrate excellent preservation of entanglement by the serrodyne transceiver proving phase-recoverable temporal multiplexing of the quantum and coherent signal within a single hybrid frequency channel.

## DISCUSSION

In conclusion, we introduced a transceiver concept enabling the transmission of quantum and coherent information via a single-frequency channel. Our approach was experimentally validated and is in excellent agreement with numerical simulations. We investigated the serrodyne dynamics of frequency-entangled photons. In judiciously chosen conditions, we demonstrated that major differences occur in the spectral dynamics of quantum and coherent signals. Our technique harnesses the random arrival time of spectrally entangled photons and the fixed arrival time of coherent pulses to enable hybrid time-multiplexed transmission of classical information and entanglement. The preservation of entanglement through the transceiver was certified via quantum state tomography of the output state. A viable serrodyne transceiver for 200-GHz channel spacing can be easily achieved via cutting-edge ultralow half-wave voltage and ultralow loss thin-film lithium niobate technology (43) and integrated microwave photonics (44). The serrodyne transceiver is conceptually simple on the basis of standard telecommunications components such as lithium niobate electro-optical phase modulators and dense-wavelength multiplexing filters and has the perspective to be fully integrated on a photonic chip. Our results demonstrate an important step toward the realization of resource-saving, hybrid quantum networks.

## MATERIALS AND METHODS

### RF waveforms

The RF waveforms were generated by an AWG (Keysight M8194A, up to 45-GHz analog bandwidth) and subsequently amplified by broadband power amplifiers (RF Lambda up to 35-GHz bandwidth, RF Lambda up to 28-GHz bandwidth). For the combined transmission of quantum and coherent signals via the serrodyne transceiver, we applied the optimized RF waveform  $\cos(ft + \alpha) \cos(\pi t/2)^{16}$  with a carrier



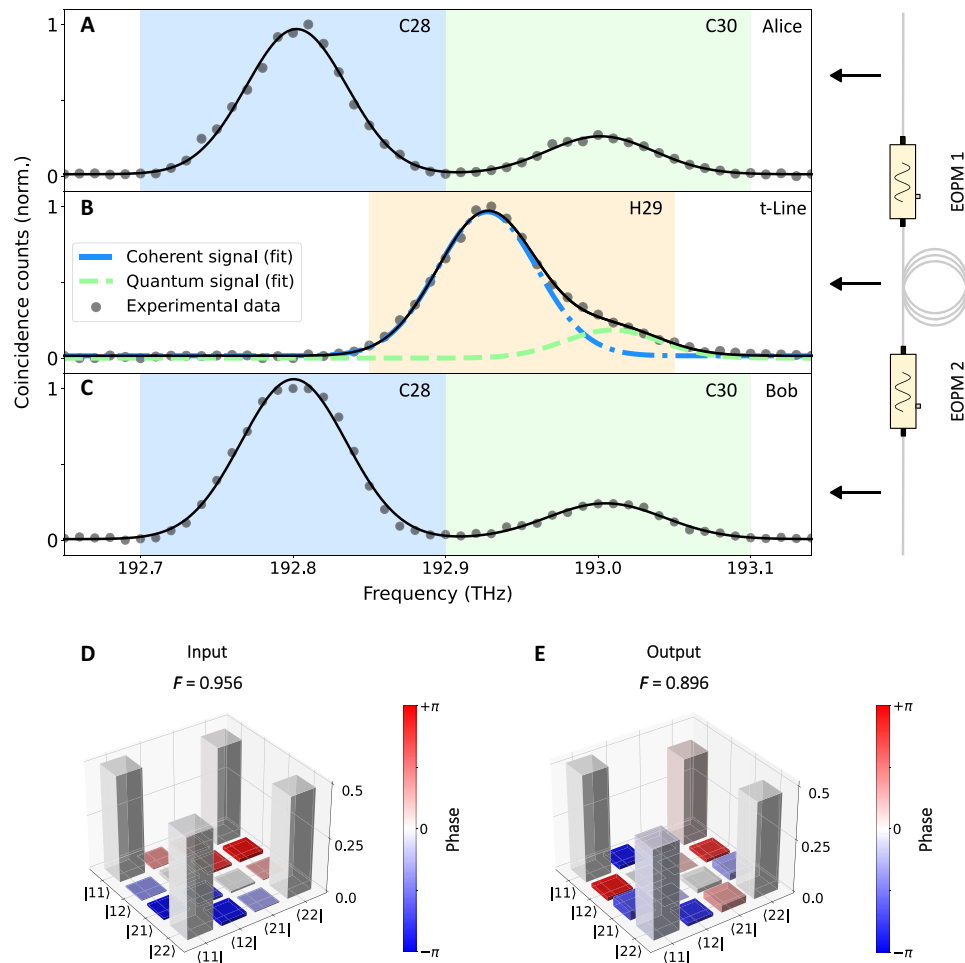


**Fig. 4. Hybrid transmission of quantum and coherent signals.** Single-photon spectra of quantum and coherent signals are displayed at three different positions in the transceiver setup. ITU frequency channels are indicated by shaded areas (C28: blue; H29: orange; C30: green). **(A)** Coherent pulses on channel C28 and quantum signal on channel C30 are shown. A bimodal Gaussian function, representing quantum and coherent light, is fitted to the measured data points (black dots). **(B)** As a guide to the eye, the individual contributions of entangled photons (green) and coherent pulses (blue), indicating the spectral overlap, are displayed. **(C)** The recovered signals, i.e., coherent pulses on C28 and quantum signal on C30 are shown. **(D and E)** Reconstructed density matrices for input and output state of the transceiver. When compared to the input state, the transmitted quantum state obtained a slight spectral phase shift ( $\approx \pi/15$ ) due to dispersion of the transceiver (DWDMs and EOPMs).

frequency of  $f/(2\pi) = 20$  GHz to the electro-optic phase modulators, where  $\alpha$  is the carrier-envelope offset phase. The envelope was chosen such that it falls off fast in frequency domain and hence is compatible with the limited gain bandwidth ( $\sim 10$  to  $28$  GHz) of the RF amplifiers used. The amplitude and phase response of the setup was characterized via electro-optical sampling (see the Supplementary Materials).

## Supplementary Materials

This PDF file includes:

Supplementary Text  
Figs. S1 to S8  
Table S1  
References

## REFERENCES AND NOTES

- H. J. Kimble, The quantum internet. *Nature* **453**, 1023–1030 (2008).
- S. Wehner, D. Elkouss, R. Hanson, Quantum internet: A vision for the road ahead. *Science* **362**, eaam9288 (2018).
- N. Gisin, R. Thew, Quantum communication. *Nat. Photonics* **1**, 165–171 (2007).
- C. Couteau, S. Barz, T. Durt, T. Gerrits, J. Huwer, R. Prevedel, J. Rarity, A. Shields, G. Weihs, Applications of single photons to quantum communication and computing. *Nat. Rev. Phys.* **5**, 326–338 (2023).
- A. S. Cacciapuoti, M. Caleffi, F. Tafuri, F. S. Cataliotti, S. Gherardini, G. Binachi, Quantum internet: Networking challenges in distributed quantum computing. *IEEE Network* **34**, 137–143 (2020).
- R. Ursin, F. Tiefenbacher, T. Schmitt-Manderbach, H. Weier, T. Scheidl, M. Lindenthal, B. Blauensteiner, T. Jennewein, J. Perdigues, P. Trojek, B. Ömer, M. Fürst, M. Meyenburg, J. Rarity, Z. Sodnik, C. Barbieri, H. Weinfurter, A. Zeilinger, Entanglement-based quantum communication over 144 km. *Nat. Phys.* **3**, 481–486 (2007).
- O. Lib, Y. Bromberg, Quantum light in complex media and its applications. *Nat. Phys.* **18**, 986–993 (2022).
- M. Kues, C. Reimer, J. M. Lukens, W. J. Munro, A. M. Weiner, D. J. Moss, R. Morandotti, Quantum optical microcombs. *Nat. Photonics* **13**, 170–179 (2019).
- H. H. Lu, M. Liscidini, A. L. Gaeta, A. M. Weiner, J. M. Lukens, Frequency-bin photonic quantum information. *Optica* **10**, 1655–1671 (2023).
- C. Bernhard, B. Bessire, T. Feurer, A. Stefanov, Shaping frequency-entangled qudits. *Phys. Rev. A* **88**, 032322 (2013).
- M. Kues, C. Reimer, P. Roztock, L. R. Cortés, S. Sciara, B. Wetzel, Y. Zhang, A. Cino, S. T. Chu, B. E. Little, D. J. Moss, L. Caspani, J. Azaña, R. Morandotti, On-chip generation of high-dimensional entangled quantum states and their coherent control. *Nature* **546**, 622–626 (2017).

12. S. Francesconi, A. Raymond, R. Duhamel, P. Filloux, A. Lemaître, P. Milman, M. I. Amanti, F. Baboux, S. Ducci, On-chip generation of hybrid polarization-frequency entangled biphoton states. *Photonics Res.* **11**, 270–278 (2023).
13. J. M. Lukens, P. Lougovski, Frequency-encoded photonic qubits for scalable quantum information processing. *Optica* **4**, 8–16 (2017).
14. A. Khodadad Kashi, M. Kues, Spectral Hong–Ou–Mandel interference between independently generated single photons for scalable frequency-domain quantum processing. *Laser Photonics Rev.* **15**, 2000464 (2021).
15. G. Moody, V. J. Sorger, D. J. Blumenthal, P. W. Juodawlkis, W. Loh, C. Sorace-Agaskar, A. E. Jones, K. C. Balram, J. C. F. Matthews, A. Laing, M. Davanco, L. Chang, J. E. Bowers, N. Quack, C. Galland, I. Aharonovich, M. A. Wolff, C. Schuck, N. Sinclair, M. Lončar, T. Komljenovic, D. Weld, S. Mookherjee, S. Buckley, M. Radulaski, S. Reitzenstein, B. Pingault, B. Machielse, D. Mukhopadhyay, A. Akimov, A. Zheltikov, G. S. Agarwal, K. Srinivasan, J. Lu, H. X. Tang, W. Jiang, T. P. McKenna, A. H. Safavi-Naeini, S. Steinhauer, A. W. Elshaari, V. Zwiller, P. S. Davids, N. Martinez, M. Gehl, J. Chiaverini, K. K. Mehta, J. Romero, N. B. Lingaraju, A. M. Weiner, D. Peace, R. Cernansky, M. Lobino, E. Diamanti, L. T. Vidarte, R. M. Camacho, 2022 roadmap on integrated quantum photonics. *J. Phys. Photonics* **4**, 012501 (2022).
16. H. Mahmudlu, R. Johanning, A. Van Rees, A. Khodadad Kashi, J. P. Epping, R. Haldar, K. J. Boller, M. Kues, Fully on-chip photonic turnkey quantum source for entangled qubit/qudit state generation. *Nat. Photonics* **17**, 518–524 (2023).
17. B. Hage, A. Sambrowski, R. Schnabel, Towards Einstein-Podolsky-Rosen quantum channel multiplexing. *Phys. Rev. A* **81**, 062301 (2010).
18. S. Wengerowsky, S. K. Joshi, F. Steinlechner, H. Hübel, R. Ursin, An entanglement-based wavelength-multiplexed quantum communication network. *Nature* **564**, 225–228 (2018).
19. K. A. Patel, J. F. Dynes, I. Choi, A. W. Sharpe, A. R. Dixon, Z. L. Yuan, R. V. Penty, A. J. Shields, Coexistence of high-bit-rate quantum key distribution and data on optical fiber. *Phys. Rev. X* **2**, 041010 (2012).
20. L. J. Wang, K. H. Zou, W. Sun, Y. Mao, Y. X. Zhu, H. L. Yin, Q. Chen, Y. Zhao, F. Zhang, T. Y. Chen, J. W. Pan, Long-distance copropagation of quantum key distribution and terabit classical optical data channels. *Phys. Rev. A* **95**, 012301 (2017).
21. Z. Yang, M. Jahanbozorgi, D. Jeong, S. Sun, O. Pfister, H. Lee, X. Yi, A squeezed quantum microcomb on a chip. *Nat. Commun.* **12**, 4781 (2021).
22. A. Pasquazi, M. Peccianti, L. Razzari, D. J. Moss, S. Coen, M. Erkintalo, Y. K. Chembo, T. Hansson, S. Wabnitz, P. Del'Haye, Y. Xue, A. M. Weiner, R. Morandotti, Micro-combs: A novel generation of optical sources. *Phys. Rep.* **729**, 1–81 (2018).
23. L. Lundberg, M. Mazur, A. Mirani, B. Foo, J. Schröder, V. Torres-Company, M. Karlsson, P. A. Andrekson, Phase-coherent lightwave communications with frequency combs. *Nat. Commun.* **11**, 201 (2020).
24. L. Shao, N. Sinclair, J. Leatham, Y. Hu, M. Yu, T. Turpin, D. Crowe, M. Lončar, Integrated microwave acousto-optic frequency shifter on thin-film lithium niobate. *Opt. Express* **28**, 23728–23738 (2020).
25. X. Zeng, W. He, M. H. Frosz, A. Geilen, P. Roth, G. K. Wong, P. S. Russell, B. Stiller, Stimulated Brillouin scattering in chiral photonic crystal fiber. *Photonics Res.* **10**, 711–718 (2022).
26. L. Fan, C. L. Zou, M. Poot, R. Cheng, X. Guo, X. Han, H. X. Tang, Integrated optomechanical single-photon frequency shifter. *Nat. Photonics* **10**, 766–770 (2016).
27. D. Zhu, C. Chen, M. Yu, L. Shao, Y. Hu, C. J. Xin, M. Yeh, S. Ghosh, L. He, C. Reimer, N. Sinclair, F. N. C. Wong, M. Zhang, M. Lončar, Spectral control of nonclassical light pulses using an integrated thin-film lithium niobate modulator. *Light Sci. Appl.* **11**, 327 (2022).
28. N. Matsuda, Deterministic reshaping of single-photon spectra using cross-phase modulation. *Sci. Adv.* **2**, e1501223 (2016).
29. P. Balla, H. Tünnermann, S. H. Salman, M. Fan, S. Alisauskas, I. Hartl, C. M. Heyl, Ultrafast serrodyne optical frequency translator. *Nat. Photonics* **17**, 187–192 (2023).
30. ITU-T Recommendation G.694.1, Spectral grids for WDM applications: DWDM frequency grid, v1.0 (2002).
31. L. J. Wright, M. Karpiński, C. Söller, B. J. Smith, Spectral shearing of quantum light pulses by electro-optic phase modulation. *Phys. Rev. Lett.* **118**, 023601 (2017).
32. M. Karpiński, M. Jachura, L. J. Wright, B. J. Smith, Bandwidth manipulation of quantum light by an electro-optic time lens. *Nat. Photonics* **11**, 53–57 (2017).
33. F. Sośnicki, M. Mikołajczyk, A. Golestani, M. Karpiński, Interface between picosecond and nanosecond quantum light pulses. *Nat. Photonics* **17**, 761–766 (2023).
34. M. Alshowkan, B. P. Williams, P. G. Evans, N. S. V. Rao, E. M. Simmerman, H. H. Lu, N. B. Lingaraju, A. M. Weiner, C. E. Marvinney, Y. Y. Pai, B. J. Lawrie, N. A. Peters, J. M. Lukens, Reconfigurable quantum local area network over deployed fiber. *PRX Quantum* **2**, 040304 (2021).
35. N. B. Lingaraju, H. H. Lu, D. E. Leaird, S. Estrella, J. M. Lukens, A. M. Weiner, Bell state analyzer for spectrally distinct photons. *Optica* **9**, 280–283 (2022).
36. L. M. Johnson, C. H. Cox, Serrodyne optical frequency translation with high sideband suppression. *J. Light. Technol.* **6**, 109–112 (1988).
37. B. Crockett, L. R. Cortés, R. Maram, J. Azaña, Optical signal denoising through temporal passive amplification. *Optica* **9**, 130–138 (2022).
38. B. Crockett, L. R. Cortés, S. R. Konatham, J. Azaña, Full recovery of ultrafast waveforms lost under noise. *Nat. Commun.* **12**, 2402 (2021).
39. H. Guillet de Chatellus, L. Romero Cortés, C. Schnébelin, M. Burla, J. Azaña, Reconfigurable photonic generation of broadband chirped waveforms using a single CW laser and low-frequency electronics. *Nat. Commun.* **9**, 2438 (2018).
40. C. Liu, S. Zhou, J. Shang, Z. Zhao, H. Gao, X. Chen, S. Yu, Stabilized radio frequency transfer via 100 km urban optical fiber link using passive compensation method. *IEEE Access* **7**, 97487–97491 (2019).
41. C. Lim, A. Nirmalathas, Radio-over-fiber technology: Present and future. *J. Light. Technol.* **39**, 881–888 (2021).
42. J. F. Clauser, M. A. Horne, A. Shimony, R. A. Holt, Proposed experiment to test local hidden-variable theories. *Phys. Rev. Lett.* **23**, 880–884 (1969).
43. M. Xu, M. He, H. Zhang, J. Jian, Y. Pan, X. Liu, L. Chen, X. Meng, H. Chen, Z. Li, X. Xiao, S. Yu, S. Yu, X. Cai, High-performance coherent optical modulators based on thin-film lithium niobate platform. *Nat. Commun.* **11**, 3911 (2020).
44. D. Marpaung, J. Yao, J. Capmany, Integrated microwave photonics. *Nat. Photonics* **13**, 80–90 (2019).
45. K. Sedziak, M. Lasota, P. Kolenderski, Reducing detection noise of a photon pair in a dispersive medium by controlling its spectral entanglement. *Optica* **4**, 84–89 (2017).
46. G. Chen, K. Chen, R. Gan, Z. Ruan, Z. Wang, P. Huang, C. Lu, A. P. T. Lau, D. Dai, C. Guo, L. Liu, High performance thin-film lithium niobate modulator on a silicon substrate using periodic capacitively loaded traveling-wave electrode. *APL Photonics* **7**, 026103 (2022).
47. Z. Wang, Z. Fang, Z. Liu, Y. Liang, J. Liu, J. Yu, T. Huang, Y. Zhou, H. Zhang, M. Wang, Y. Cheng, On-chip arrayed waveguide grating fabricated on thin-film lithium niobate. *Adv. Photonics Res.* **5**, 2300228 (2024).
48. J. A. Valdmann, G. Mourou, C. W. Gabel, Picosecond electro-optic sampling system. *Appl. Phys. Lett.* **41**, 211–212 (1982).
49. H. H. Lu, J. M. Lukens, N. A. Peters, O. Odele, D. E. Leaird, A. M. Weiner, P. Lougovski, Electro-optic frequency beam splitters and tritters for high-fidelity photonic quantum information processing. *Phys. Rev. Lett.* **120**, 030502 (2018).
50. J. Capmany, C. R. Fernández-Pousa, Quantum model for electro-optical phase modulation. *J. Opt. Soc. Am. B* **27**, A119–A129 (2010).
51. D. F. V. James, P. G. Kwiat, W. J. Munro, A. G. White, Measurement of qubits. *Phys. Rev. A* **64**, 052312 (2001).
52. B. H. Kolner, Space-time duality and the theory of temporal imaging. *IEEE J. Quantum Electron.* **30**, 1951–1963 (1994).

# Acknowledgments

**Funding:** This project was funded by the German Federal Ministry of Education and Research, Quantum Futur Program (PQuMAL), and the European Research Council (ERC) under the European Union's Horizon 2020 research and innovation programme under grant agreement no. 947603 (QFreC project), and the Deutsche Forschungsgemeinschaft (DFG, German Research Foundation) under Germany's Excellence Strategy within the Cluster of Excellence PhoenixD (EXC 2122, project ID 390833453). **Author contributions:** P.R. and J.H. conceived and designed the experiment. Experiments were conducted by J.H. and P.R. J.H. set up and characterized the photon-pair source. The RF waveform design and the electro-optical sampling were performed by P.R. The data were analyzed by P.R. and J.H. with input from R.J. and M.K. The initial draft of the manuscript was written by P.R. All authors contributed to the preparation of the final manuscript. The project was supervised by M.K. **Competing interests:** The authors declare that they have no competing interests. **Data and materials availability:** All data needed to evaluate the conclusions in the paper are present in the paper and/or the Supplementary Materials.

Submitted 5 January 2024

Accepted 21 June 2024

Published 26 July 2024

10.1126/sciadv.adn8907